Impact of water mass mixing on the biogeochemistry and microbiology of the Northeast Atlantic Deep Water

Thomas Reinthaler,[1,2] Xosé Antón Álvarez Salgado,[3] Marta Álvarez,[4]
Hendrik M. van Aken,[5] and Gerhard J. Herndl [1,6]

[1]   The extent to which water mass mixing contributes to the biological activity of the dark ocean is essentially unknown. Using a multiparameter water mass analysis, we examined the impact of water mass mixing on the nutrient distribution and microbial activity of the Northeast Atlantic Deep Water (NEADW) along an 8000 km long transect extending from 62°N to 5°S. Mixing of four water types (WT) and basin scale mineralization from the site where the WT where defined to the study area explained up to 95% of the variability in the distribution of inorganic nutrients and apparent oxygen utilization. Mixing-corrected average O_2:N:P mineralization ratios of $127(\pm11):13.0(\pm0.7):1$ in the core of the NEADW suggested preferential utilization of phosphorus compounds while dissolved organic carbon mineralization contributed a maximum of 20% to the oxygen demand of the NEADW. In conjunction with the calculated average mineralization ratios, our results indicate a major contribution of particulate organic matter to the biological activity in the NEADW. The variability in prokaryotic abundance, high nucleic acid containing cells, and prokaryotic heterotrophic production in the NEADW was explained by large scale (64–79%) and local mineralization processes (21–36%), consistent with the idea that deep-water prokaryotic communities are controlled by substrate supply. Overall, our results suggest a major impact of mixing on the distribution of inorganic nutrients and a weaker influence on the dissolved organic matter pool supporting prokaryotic activity in the NEADW.

1.   Introduction

[2]   The formation of cold dense waters in the Labrador and Greenland-Iceland-Norwegian Sea and the large-scale southward transport of North Atlantic Deep Water (NADW) drives the thermohaline circulation of the world's oceans, which plays a decisive role in the regulation of the Earth's climate [*Bryden et al.*, 2005]. Accompanied with the formation of the NADW at a rate of about 17 Sverdrup [*Smethie et al.*, 2000] is the export of relatively fresh dissolved organic matter (DOM) from the surface layer into the mesopelagic

Additional supporting information may be found in the online version of this article.

[1]Department of Limnology and Oceanography, University of Vienna, Vienna, Austria.

[2]Department of Marine Biology, University of Vienna, Vienna, Austria.

[3]Instituto de Investigaciones Marinas (IIM-CSIC), Vigo, Spain.

[4]Instituto Español de Oceanografía (IEO), A Coruña, Spain.

[5]Department of Physical Oceanography, Royal Netherlands Institute for Sea Research (NIOZ), Den Burg, Netherlands.

[6]Department of Biological Oceanography, Royal Netherlands Institute for Sea Research (NIOZ), Den Burg, Netherlands.

Corresponding author: T. Reinthaler, Department of Limnology and Oceanography, University of Vienna, Althanstrasse 14, Vienna, AT-1090, Austria. (thomas.reinthaler@univie.ac.at)

and bathypelagic realms [*Carlson et al.*, 2010]. Other than particulate organic material (POM) that is capable of sinking, the vertical transport of DOM mainly depends on convective overturning and mixing of water masses. Thus, considering the constrained direct input of DOM from the surface to the deep waters, any increase or decrease of metabolically utilizable substrates for prokaryotes in the deeper strata of the water column is largely due to the solubilization of POM and mineralization of the available and steadily aging DOM during the evolution of the NADW in the global conveyor belt [*Nagata et al.*, 2000].

[3]   In general, the mineralization of DOM derived from POM is mediated by the abundant prokaryotes. The modern view of the microbial community comprising an active component [*Herndl et al.*, 2005; *Reinthaler et al.*, 2006] contrasts with the previous idea of slow-growing prokaryotes in the dark ocean [*Jannasch and Taylor*, 1984]. Although some authors indicated a highly reduced potential for heterotrophic productivity due to pressure effects and the highly refractory nature of the DOM pool in the dark ocean when compared to the surface layer [*Bauer et al.*, 1992; *Turley*, 1993; *Tamburini et al.*, 2013], on longer time scales, prokaryotes determine to a large extent the distribution and stoichiometry of the inorganic material in the dark ocean [*Nagata et al.*, 2010].

[4]   The decrease in dissolved organic carbon (DOC) and oxygen concentrations in the individual deep water masses
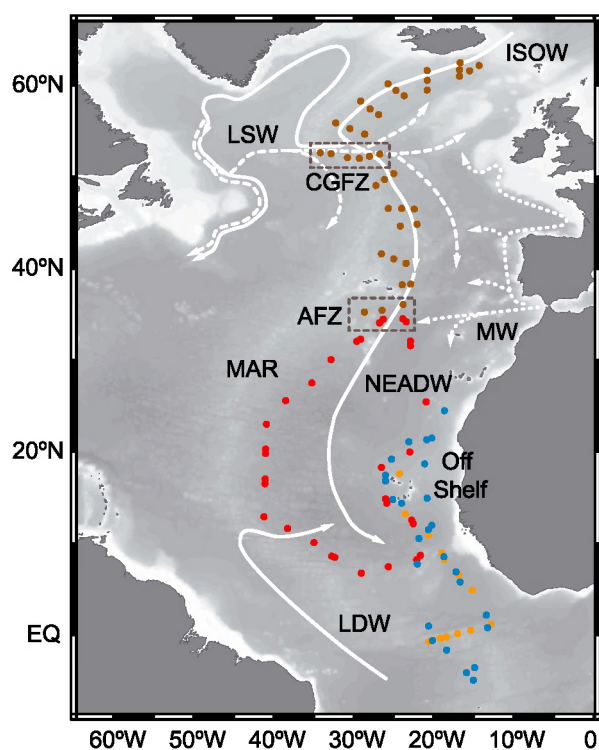
Figure 1. Occupied stations tracking the Northeast Atlantic Deep Water (NEADW). The flow of the main water masses encountered in the deep North Atlantic is indicated by white lines. Cruises were conducted in fall of the years 2002 (brown dots), 2005 (red dots), 2006 (blue dots), and 2007 (orange dots). Abbreviations of water masses see text. CGFZ: Charlie-Gibbs Fracture Zone; AFZ: Azores Frontal Zone; MAR: Mid-Atlantic Ridge.

as they age in the thermohaline circulation is an important indicator for heterotrophic metabolic activity of prokaryotes [*Bendtsen et al.*, 2002]. Comparing the DOC decrease with the decrease in oxygen concentrations indicated that the contribution of DOC to dark ocean respiration is only about 10–20% [*Arístegui et al.*, 2002; *Carlson et al.*, 2010]. Most of the DOC in the dark ocean is refractory (> 90%) which is reflected by its radiocarbon age of > 4000 years [*Williams and Druffel*, 1987; *Bauer et al.*, 1992]. However, the DOC may be differentiated into four pools in the dark ocean: a pool of semilabile DOC with a lifetime of 1.5 years, a pool of semirefractory DOC with a lifetime of 20 years, a pool of refractory DOC with a lifetime of 14,000 years, and an ultrarefractory pool with a lifetime of 40,000 years [*Hansell*, 2013]. Consequently, it is the semilabile and semirefractory DOC components that may eventually be assimilated by prokaryotes.

[5] Acknowledging the deficiencies in methodology and parameters influenced by different time and spatial scales, several recent reports point to major discrepancies between the available organic matter and the apparent metabolic requirements of the deep ocean prokaryotic community [*Reinthaler et al.*, 2006; *Steinberg et al.*, 2008; *Burd et al.*, 2010; *Reinthaler et al.*, 2010]. These studies show that the carbon demand of prokaryotes is orders of magnitude higher than the export primary production. The conversion of POM to DOM via extracellular ectoenzymes is the main mechanism

for prokaryotes to obtain assimilable substrates. Thus, part of the DOM in the dark ocean must result from the cleavage of sinking organic matter particles and aggregates apart from the DOC injected into the dark ocean during water mass formation and convective overturn at lower latitudes [*Baltar et al.*, 2009]. *Hansell et al.* [2009] estimated that ~80% of organic matter transported from the surface to the deep ocean is in the form of POM with the remainder being DOM.

[6] In this respect, analyzing the stoichiometry of the major biogenic elements in the oceans is a useful tool to assess the mineralization of organic matter in the framework of the biological pump [*Anderson and Sarmiento*, 1994]. While *Anderson and Sarmiento* [1994] considered that mineralization ratios are essentially constant with depth and basin, suggesting that large, fast-sinking phytoplankton-derived material of Redfieldian elemental composition is exported from the surface ocean and consumed in all the depth horizons, other authors concluded that there are remarkable changes in the nutrient mineralization ratios in the deep waters of the different ocean basins [*Li and Peng*, 2002] or different depths within the same basin [*Shaffer et al.*, 1999]. However, the estimation of nutrient regeneration ratios from dissolved nutrient concentrations can be distorted by the method used to eliminate the effect of the conservative mixing of water masses with different initial nutrient concentrations [*Schneider et al.*, 2005]. Direct measurements of microbial activity by prokaryotes in the dark ocean, however, are not implemented in models on DOM and/or POM mineralization, one reason being the lack of data on the conversion efficiency from particulate to dissolved organic matter by microbes.

[7] Here we study the deep pelagic realm of the NE Atlantic basin from 60°N to the equator following the core of Northeast Atlantic Deep Water (NEADW) (Figure 1). This core is identified as a deep vertical salinity maximum at about $\sigma_3 = 41.42$ or 2700 dbar [*van Aken*, 2000] in between the overlying lower salinity Labrador Sea Water (LSW) and underlying Lower Deep Water (LDW). The linear trend in the potential temperature-salinity relationship for the NEADW [*Mantyla*, 1994] derives from the sluggish circulation below 2500 dbar in the NE Atlantic basin, although some coherent patterns are discernable as an eastward current over the Mid-Atlantic Ridge (MAR) at the Charlie-Gibbs Fracture Zone (CGFZ), a southward slope current near the MAR and the continental slope of Africa [*Paillet and Mercier*, 1997] over a general cyclonic deep and abyssal circulation [*Reid*, 1994].

[8] The NEADW is a body of water defined by mixing of four water types (WT), each one characterized by a unique combination of thermohaline and chemical property values. When these properties are taken in the source region of the WT, it is called a source water type (SWT). The four WT that contribute to NEADW are Labrador Sea Water (LSW), Iceland-Scotland overflow water (ISOW), Mediterranean Water (MW), and Lower Deep Water (LDW) [*van Aken*, 2000]. LSW is a proper SWT but ISOW, MW, and LDW are WT. The property values of the ISOW were taken at the sills between Iceland and Scotland, where it forms by entrainment of the Norwegian overflow. MW was defined at about 1000 m in the Gulf of Cadiz after the intense mixing of the eastern North Atlantic central water with the Mediterranean overflow water that spills at the Strait of Gibraltar. The properties of the LDW were taken at the entry of the Vema Channel at 11°N of the Mid-Atlantic Ridge (see Table S1 in the supporting information).

[9] If NEADW would be a distinct water mass transported through the deep NE Atlantic with negligible mixing, then the O_2:C:N:P stoichiometry of the mineralization of biogenic materials could be assessed by simply comparing the dissolved oxygen and nutrient distributions. However, the previously described WT contribute to the salinity maximum of the NEADW [*van Aken*, 2000]. We hypothesized that the mixing WT does not only mask the latitudinal and longitudinal patterns of variability of nutrient mineralization but also prokaryotic activity that is intrinsic to the pure NEADW. We used a multiparameter water mass modeling approach that is based on predefined WT and thus allows calculating the proportions of the different WT influencing the NEADW. The ultimate goal was to explore the link between prokaryotic biomass and activity and nutrient mineralization and stoichiometry along the NEADW core in the NE Atlantic basin that is corrected for water mass mixing and hence yielding a better approximation of microbe-mediated biogeochemical cycling in the NEADW.

2. Methods

2.1. Sampling Methodology

[10] Four cruises were conducted in the eastern basin of the North Atlantic spanning a transect from 62°N to 5°S. The cruises were carried out in the fall of the years 2002 (60°N–25°N), 2005, 2006, and 2007 (25°N–5°S) (Figure 1) resulting in a total number of 113 stations relevant for the current analysis. The stations sampled in the subtropical Atlantic at the different cruises were only partly overlapping. At 5 depth levels, discrete seawater samples for physicochemical and biological parameters were taken from 10 L Niskin bottles mounted on a Seabird conductivity-temperature-depth rosette (for details of sampled depth levels, see Table S2). Water masses were identified on board using downcast records of conductivity (salinity) and temperature [*van Aken*, 2000]. Initial readings of the conductivity, temperature, pressure, and oxygen (SBE 43, Seabird Electronics) were calibrated and passed World Ocean Circulation Experiment requirements [*WOCE operations manual*, 1994]. The derived parameters of potential temperature (θ) and apparent oxygen utilization (AOU) were calculated using the algorithms implemented in the software package Ocean Data View 4.4.2 [*Schlitzer*, 2002].

2.2. Nutrient Measurements

[11] Nutrient measurements followed standard segmented flow analysis with Joint Global Ocean Flux Study recommendations [*Gordon et al.*, 1993]. The concentrations of NH_4, NO_2, NO_3, PO_4, and SiO_4 were determined on a continuous flow autoanalyzer (Technicon TRAACS 800) immediately after collecting the samples and gentle filtration through 0.2 μm Acrodisc filters. Total dissolved nitrogen and total dissolved phosphorus were analyzed following the persulfate oxidation method as described in *Kramer et al.* [2005] (for details and detection limits, see supporting information Material and Methods).

2.3. DOC Measurements

[12] DOC was measured as unfiltered total organic carbon from samples that were transferred directly from the Niskin bottles into duplicate 8 mL precombusted amber glass ampoules. The ampoules were heat sealed after acidification to pH < 2 with phosphoric acid and stored frozen at -20°C until analysis back in the lab. DOC analysis was performed using the high-temperature combustion method on a Shimadzu TOC-5000A. Quadruplicate sample injections compared to a three-point standard curve, prepared with potassium hydrogen phthalate, were used to calculate DOC concentrations. The instrument's performance and the validity of the calibration were determined using reference material of the Hansell consensus reference materials program (44–46 μmol L^{-1} for the reference samples; n = 3 and 1–2 μmol L^{-1} for low carbon water; n = 3). The average analytical precision of the instrument was < 3%.

2.4. Prokaryotic Abundance

[13] Counts of prokaryotic abundance (PA) broadly followed the protocol of *Gasol et al.* [1999]. For each sample, 1 mL of unfiltered seawater sample was fixed with 37% of 0.2 μm filtered formaldehyde (2% final concentration), incubated for 10 min at room temperature in the dark, and stored frozen in liquid nitrogen. Prior to the analysis, samples were thawed and stained with 10 μL of SYBR Green I (Molecular Probes) of a 1:200 dilution of the stock solution and incubated in the dark for 15 min. Prokaryotic cells were enumerated with an on board FACSCalibur flow cytometer (BD Biosciences) using the excitation of the argon laser line at 488 nm and scatterplots of right angle light scatter versus green fluorescence measured at 530 nm. Counts were calibration with fluorescent microspheres (Molecular Probes) of 1 μm diameter added to all samples. Data were acquired in log mode until 10,000 events were registered. High nucleic acid (HNA) prokaryotes were distinguished from low nucleic acid (LNA) cells in the side scatter versus green fluorescence plot where HNA populations show higher fluorescence compared to LNA cells (see Figure S1). Prokaryotic carbon biomass (PB) was calculated assuming a carbon content of 10 fg C $cell^{-1}$ [*Ducklow et al.*, 2000].

2.5. Prokaryotic Heterotrophic Production

[14] Prokaryotic heterotrophic production (PHP) of the unfiltered seawater was measured by ^{3}H-leucine incorporation (specific activity: 595.7×10^{10} Bq $mmol^{-1}$; final concentration 5–10 nmol L^{-1}) and followed the method described in *Reinthaler et al.* [2010]. Three 10–40 mL samples and three blanks were incubated in the dark. The blanks were fixed with concentrated 0.2 μm filtered formaldehyde (4% final concentration, v/v) 10 min prior to adding the tracer. After incubating the samples and the blanks at in situ temperature for 4–48 h, depending on the expected activity, the samples were fixed with formaldehyde (4% final concentration), filtered onto 0.2 μm polycarbonate filters using nitrocellulose supporting filters, and rinsed twice with 5 mL ice cold 5% trichloroacetic acid for 5 min. Thereafter, the filters were transferred to 20 mL scintillation vials and the filters were allowed to dry. Subsequently, 8 mL of scintillation cocktail (Filter Count, Perkin-Elmer) was added and after 18 h, the radioactivity counted in a liquid scintillation counter. Leucine incorporated into prokaryotic biomass was converted to carbon production using the theoretical conversion factor of 1.55 kg C mol^{-1} leucine assuming no isotope dilution [*Simon and Azam*, 1989].

2.6. Multiparameter Water Mass Analysis

[15] Briefly, the proportions of the four water types (MW, LSW, ISOW, and LDW) contributing to the NEADW were
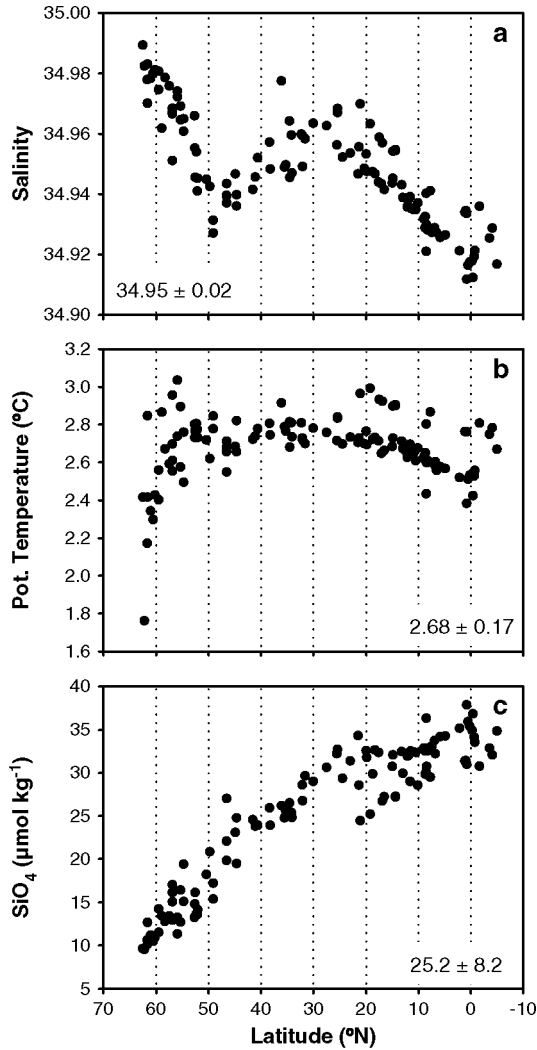
Where N_j is the measured concentration of N in sample j. N_i, the adjustable parameters, are the expected concentrations of N in WT i. Note that whereas the water type values of conservative parameters (θ, S, and SiO_4) retain the conditions in the area where they were defined, the water type values of nonconservative parameters retain the variability due to both: (i) the conditions in the area where they were defined (i.e., the initial preformed concentrations) and (ii) the mineralization of biogenic materials from the area of definition to the center of mass of each water type in the study area [*Perez et al.*, 1993; *Álvarez-Salgado et al.*, 2013]. A system of 113 linear mixing equations (one per sample) with four unknowns, N_i (one per WT) was solved by minimizing the residuals of these equations in a least squares sense. The higher the correlation coefficient (r^2) and the lower the standard deviation of the residuals (SD) of the least squares analysis, the larger the impact of WT mixing on the distribution of parameter N. Local biogeochemical variability, i.e., biogeochemical differences between samples with the same WT composition, is contained in the residuals of equation (1), which represent the proportion of N that cannot be modeled just by WT mixing.

[18] In summary, the relationship between any pair of nonconservative parameters (N_1, N_2), either geochemical or microbial, depends upon (i) conservative mixing of WT with contrasting N_i values and (ii) nonconservative biogeochemical processes that occur during that mixing, both at the basin scale (from the area where they were defined to the center of mass of each WT in the study area) and the local scale (different processes or intensities of the same processes in samples of the same WT composition). Thus, the following equation allows modeling the relationship between N_1 and N_2:

$$N_{1j} - \sum_i x_{ij}\cdot N_{1i} = \beta\cdot\left(N_{2j} - \sum_i x_{ij}\cdot N_{2i}\right) \quad \text{or}$$

$$N_{1j} = \sum_i x_{ij}\cdot(N_{1i} - \beta\cdot N_{2i}) + \beta\cdot N_{2j} \quad j = 1 \text{ to } 113 \text{ samples} \tag{2}$$

Where N_{1j} and N_{2j} are the concentrations of N_1 and N_2 in sample j. N_{1i} and N_{2i} are the adjustable WT concentrations of N_1 and N_2, respectively. β is the adjustable coefficient of the relationship between parameters N_1 and N_2, which is independent of the mixing and models the local-scale mineralization. Again, a system of 113 linear mixing equations (one per sample) was solved with 5 unknowns, in this case four parameters (one per WT) and β. As for the case of equation (1), the goodness of this linear physical-biogeochemical parametric model was tested using the correlation coefficient (r^2) and the standard error of the residuals of the least squares analysis. Furthermore, to assess the robustness of the estimated β, we performed a perturbation test of equation (2) following the previously referred method of *Lawson and Hanson* [1974] in which the values of N_1, N_2, and x_{ij} were modified, introducing normally distributed random numbers within the uncertainties of their respective estimates: the analytical errors in the case of N_1 and N_2 and the standard deviation of the results of the 100 perturbation experiments previously conducted to obtain the water mass proportions in the case of x_{ij}.

Figure 2. Observed latitudinal gradients of physicochemical parameters in the NEADW core. (a) Salinity, (b) potential temperature (°C), and (c) silicate (SiO_4; $\mu mol\,kg^{-1}$) along the transect from 70°N to 10°S. Numbers in the inset indicate average ± standard deviation over the transect.

objectively quantified by solving a set of linear mixing equations of potential temperature (θ), salinity (S), and silicate (SiO_4) conservation with the constraint that the contributions of all WT must be positive and sum up to 100% [*Brea et al.*, 2004] (for details, see supporting information Material and Methods).

[16] The θ, S, and SiO_4 of the water types used in the analysis (see Table S1) is based upon previous studies in the area [*van Aken*, 2000; *Alvarez et al.*, 2004; *Álvarez-Salgado et al.*, 2013]. Furthermore, we assume that these tracers behave conservatively in the deep NE Atlantic basin. The robustness of the estimation of the water mass proportions was assessed using a perturbation test according to *Lawson and Hanson* [1974] (for details, see supporting information Material and Methods).

[17] After calculating the WT proportions contributing to each sample, the concentration of any nonconservative parameter, N, was modeled by calculating the parameters that better fit the equation:

$$N_j = \sum_i x_{ij}\cdot N_i \quad j = 1 \text{ to } 113 \text{ samples} \tag{1}$$

2.7. Conversion of O_2:N:P Molar Ratios Into Biochemical Marine Phytoplankton Composition

[19] Assuming that changes in the O_2:C:N:P stoichiometry of the oceans are due to variations in the proportions of
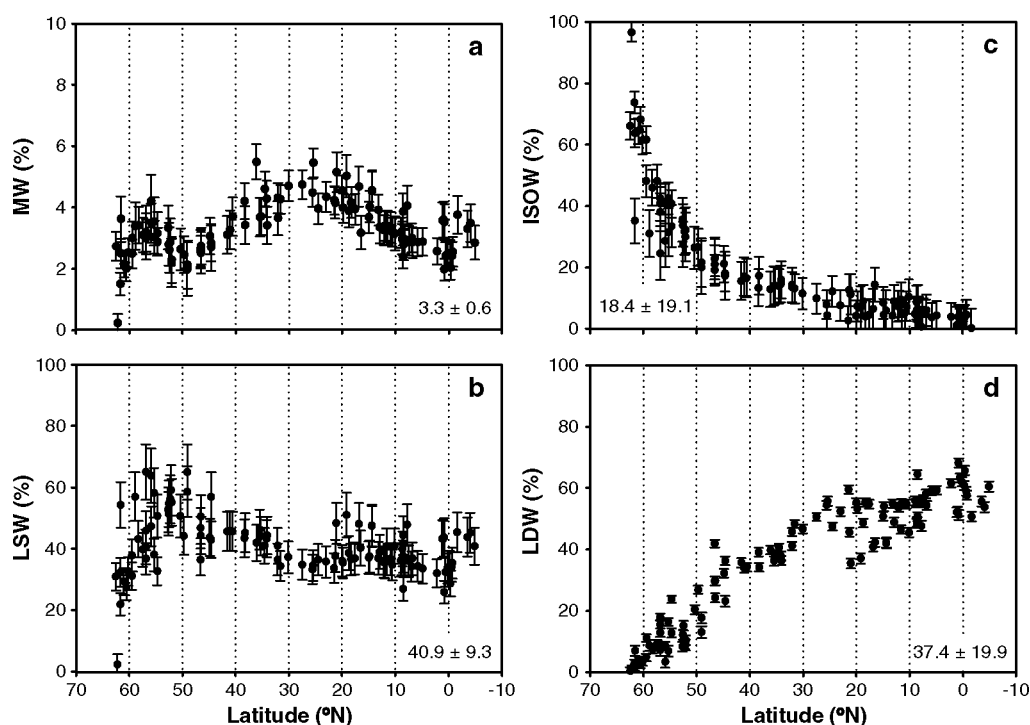
Figure 3. Proportions of water types contributing to the NEADW core as calculated using multiparameter water mass analysis. The percent contributions of (a) Mediterranean Water (MW), (b) Labrador Sea Water (LSW), (c) Iceland-Scotland Overflow Water (ISOW), and (d) Lower Deep Water (LDW) along the transect from 70°N to 10°S are indicated by dots. Error bars indicate standard deviations from the perturbation analysis. Numbers in the inset indicate average ± standard deviation over the transect.
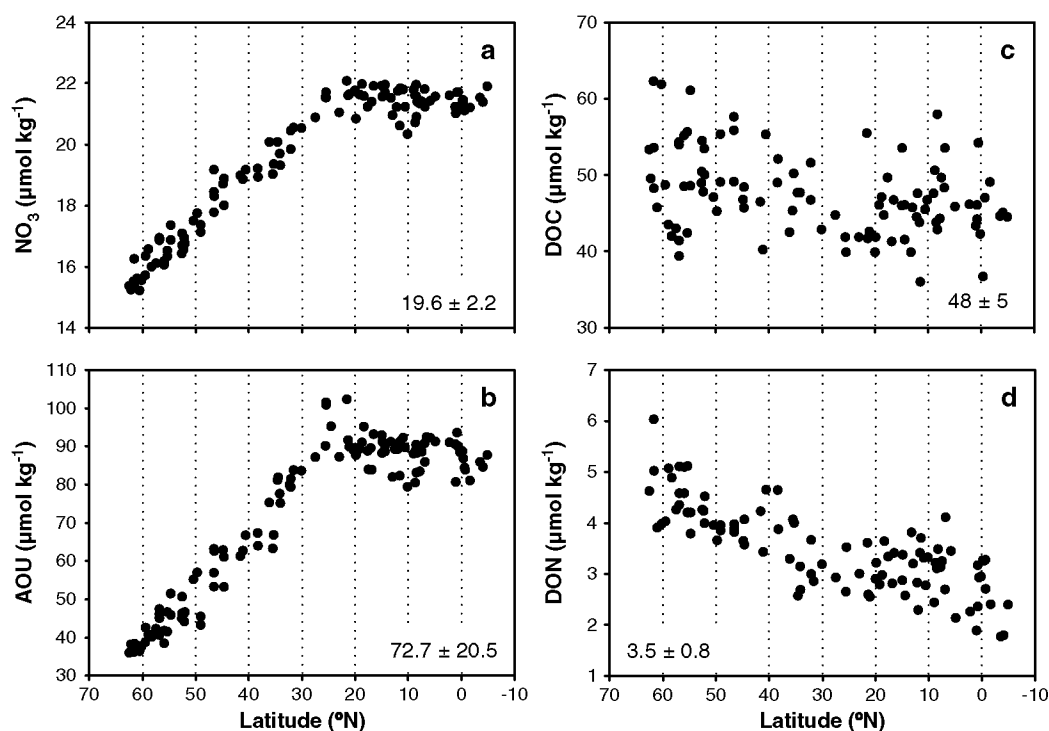

Figure 4. Observed latitudinal gradients of chemical parameters in the NEADW core. (a) Nitrate (NO_3; $\mu mol\, kg^{-1}$), (b) apparent oxygen utilization (AOU; $\mu mol\, kg^{-1}$), (c) total organic carbon (DOC; $\mu mol\, kg^{-1}$), and (d) dissolved organic nitrogen (DON; $\mu mol\, kg^{-1}$) along the transect from 70°N to 10°S. Numbers in the inset indicate average ± standard deviation over the transect.
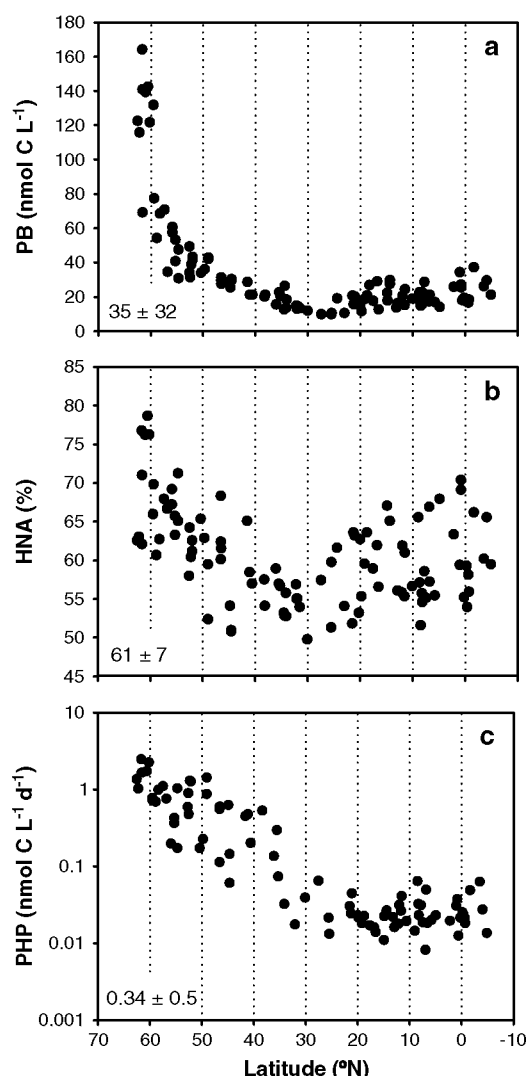
Figure 5. Observed latitudinal gradients of prokaryotic biomass and activity in the NEADW core. (a) Prokaryotic biomass (PB; nmol C L^{-1}), (b) high nucleic acid-containing cells (HNA, %), and (c) prokaryotic heterotrophic production (PHP, nmol C L^{-1} d^{-1}). Note that the y axis in Figure 5b is log transformed. Numbers in the inset indicate average ± standard deviation over the transect.

the products of synthesis and early degradation of marine phytoplankton, i.e., carbohydrates, lipids, proteins and phosphorus compounds, rather than variations in the molecular ratio of each group [*Álvarez-Salgado et al.*, 2006], we estimated their proportions as stated by *Fraga et al.* [1998] (see supporting information Material and Methods and Table S3).

3. Results

3.1. Latitudinal Gradients of Physicochemical Parameters and SWT Proportions in the NEADW Core

[20] The NEADW core was identified by a conspicuous relative vertical salinity maximum at about 2700 m depth at each of our 113 stations. The highest salinity (34.98)

and lowest potential temperature (1.76°C) at the northern end of the study area pointed to the major contribution of Iceland-Scotland Overflow Water (ISOW) to NEADW (Figures 2a and 2b). In fact, the contribution of the ISOW (mean ± sd: 18.4 ± 19.1%) decreased exponentially toward the equator from ~96% at > 60°N to 5% in the subtropical North Atlantic (Figure 3c).

[21] A relative salinity minimum of ~34.93 was encountered near the entrance of the Charlie-Gibbs Fracture Zone (CGFZ; 48–52°N), a major conduit of the LSW originating in the western basin of the Atlantic (Figure 2a). At the CGFZ, the contribution of the LSW (mean ± sd: 40.9 ± 9.3%) peaked with proportions of around 62% and was rather stable toward the south with contributions of ~40% to the NEADW core (Figure 3b).

[22] At the latitudinal range of the Strait of Gibraltar (34.5°N–25.5°N), the highest influence of the MW of 5.2% led to an increase in NEADW salinity to 34.96 (Figures 2a and 3a). Overall, the contribution of the MW was low and on average 3.3 ± 0.6% (mean ± sd).

[23] South of 30°N, the influence of LDW (Figure 3d) led to a decrease in the salinity of the NEADW (Figure 2a) and an increase in silicate concentrations (Figure 2c). The LDW contribution (mean ± sd: 37.4 ± 19.9%) increased from 3% in the northern North Atlantic to ~60% near the equatorial Atlantic (Figure 3d).

[24] NO_3 (Figure 4a) and PO_4 concentrations (not shown) ranged from 15.2–22.1 μmol N kg^{-1} and 1.0–1.6 μmol P kg^{-1}, respectively. Both increased almost linearly southward toward 25°N, where they reached highest and essentially constant concentrations between 25°N and 5°S. Dissolved inorganic nitrogen mainly consisted of NO_3 (> 99%), whereas NO_2 did not exhibit any latitudinal trend (data not shown). Coinciding with the increasing influence of LDW, higher silicate concentrations were detected toward the south of our study region, increasing monotonically from 9.6 μmol Si kg^{-1} at the northern end of the transect to 37.9 μmol Si kg^{-1} at the equator (Figure 2c).

[25] Similar to the distribution of inorganic nutrients, the AOU increased from 35.9 μmol O_2 kg^{-1} at the northernmost station to a maximum of 90.1 ± 16.1 μmol O_2 kg^{-1} from ~25°N southward (Figure 4b). DOC concentrations were in the range of 39–62 μmol C kg^{-1} (mean ± sd: 48 ± 5 μmol kg^{-1}) and decreased significantly ($p < 0.0001$, $n = 91$) toward the equator (Figure 4c).

[26] Dissolved organic nitrogen (DON) decreased linearly toward the south from 5.1–1.8 μmol N kg^{-1} (mean ± sd: 3.5 ± 0.8 μmol N kg^{-1}) (Figure 4d). DON comprised between 7 and 30% of the total dissolved N pool with decreasing proportions toward the equator. DOP exhibited a large scatter along the transect ranging from 0.04–0.18 μmol P kg^{-1} (mean ± sd: 0.10 ± 0.03 μmol kg^{-1}; $n = 72$) representing 6.5% of the total dissolved P pool (data not shown).

3.2. Latitudinal Gradients of Prokaryotic Biomass and Heterotrophic Production in the NEADW Core

[27] Prokaryotic biomass (PB) decreased exponentially toward the south from 164 to 10 nmol C L^{-1} and was rather stable south of 36°N with an average biomass of 19 ± 6 nmol C L^{-1} (overall mean ± sd: 35 ± 32 nmol C L^{-1}, $n = 107$; Figure 5a). The fraction of HNA cells decreased by roughly 30% from the north toward the Azores region (~36°N) and

Table 1. Least Squares Regression Results of the Mixing-Model Applied Along the NEADW Core[a]

Parameter[b]	Unit	LSW	ISOW	LDW	r^{2c}	SD[d]	n[e]	p[f]	Var (%)[g]
AOU	μmol kg^{-1}	15±4	26±3	118±3	0.95	4.8	113	< 0.001	5
PO$_4$	μmol kg^{-1}	1.00±0.03	0.95±0.02	1.64±0.02	0.93	0.04	113	< 0.001	7
NO$_3$	μmol kg^{-1}	15.1±0.4	13.8±0.3	24.4±0.3	0.95	0.49	113	< 0.001	5
DOP	μmol kg^{-1}	0.14±0.03	0.08±0.02	0.12±0.03	0.18	0.04	82	< 0.225	–
DON	μmol kg^{-1}	3.8±0.5	6.3±0.3	2.6±0.3	0.63	0.5	100	< 0.001	37
DOC	μmol kg^{-1}	60±4	53±3	45±3	0.30	4.0	91	< 0.001	70
PA[h]	cells mL^{-1}	0.0±0.2	2.0±0.1	0.3±0.1	0.79	0.18	104	< 0.001	21
HNA[h]	cells mL^{-1}	0.0±0.1	1.4±0.1	0.2±0.1	0.76	0.14	104	<0.001	24
PHP	nmol C L^{-1} d^{-1}	0.7±0.3	2.0±0.2	0.0±0.2	0.64	0.31	91	< 0.001	36

[a]From equation (1). Values ± SE represent coefficients of chemical and biological parameters (N_j) of each SWT.
[b]Abbreviations of parameters and water masses see text.
[c]Coefficient of determination, indicates the total variability of the parameter accounted for by SWT mixing.
[d]Standard deviation of the residuals.
[e]Number of data.
[f]p value indicating significant regression model.
[g]Percentage of the variance accounted for by biogeochemical processes (Var = $1 - r^2 \times 100$) for each variable along the NEADW core.
[h]Prokaryotic abundance × 10^5.

subsequently increased again toward the equator. Overall, the contribution of HNA cells to the total prokaryotic abundance was rather stable with an average of 61 ± 7% ($n = 107$; Figure 5b). Prokaryotic heterotrophic production (PHP) revealed a similar pattern as PB and decreased from the north to 36°N from 1.46 to 0.01 nmol C L^{-1} d^{-1}. In the subtropical Atlantic toward 5°S, PHP was variable with an average of 0.03 ± 0.01 nmol C L^{-1} d^{-1} (Figure 5c). The increasing inorganic nutrient concentrations from North to South coincided with decreasing PB and PHP. Prokaryotic growth rates decreased southward and was 0.020 ± 0.008 d^{-1} north of 36°N (turnover time: 93 ± 66 d) and 0.002 ± 0.001 d^{-1} under the subtropical gyre south of 36°N (turnover time: 775 ± 325 d; data not shown).

4. Discussion

4.1. Choice of Model

[28] There are several parametric inverse models that can be used to analyze the mineralization of organic matter in the dark ocean. Most approaches rely on the assumption that mixing occurs strictly on isopycnal surfaces [*Takahashi et al.*, 1985; *Hansell and Carlson*, 2001; *Li and Peng*, 2002]. We have used a multiparameter inverse model that accounts for both, diapycnal and isopycnal mixing, as a relatively simple approach to separate the contribution of the different water types that mix to form a water mass. Other than defining the initial WT properties, no further a priori assumptions on the sources and sinks of constituents are needed for the data analysis, and thus, the method lends itself to be extended to biological data. A potential source of bias in the multiparameter inverse model is its sensitivity to the definition of the end-members needed for the mixing analysis. By carefully selecting the end-member properties, the analysis has been shown to compare well to more complex models of ocean carbon cycling [*Schneider et al.*, 2005]. By means of a perturbation test, we have also shown that the variability of θ, S, and SiO$_4$ in the areas where the four water types that contribute to the NEADW were defined did not substantially affect the results of the model; the average error of the estimation of the WT proportions was generally low and ~1% for the MW and LDW and ~6% for the ISOW and LSW (Figure 3).

4.2. Impact of Conservative Mixing Versus Nonconservative Biogeochemical Processes on Dissolved Oxygen and Inorganic Nutrients

[29] Based on the proportions of the four water types forming the NEADW (Figure 3), our model explained 93–95% of the total variability of dissolved oxygen and inorganic nutrient concentrations (see r^2 in Table 1), suggesting that conservative mixing and basin-scale mineralization are the main factors explaining the variability of these parameters along the NEADW core. Although the variability not explained by equation (1) is only 5–7% (see Var% in Table 1), the standard deviation of the residuals of the mixing model of these variables (see SD in Table 1) is about an order of magnitude larger than the corresponding analytical errors (see section 2). Therefore, the impact of local-scale nonconservative biogeochemical processes is still considerable. The distribution of the residuals allows obtaining further insights into mechanisms causing this variability.

[30] The WT values of AOU (N_i in equation (1)) in Table 1 are significantly larger than 0. Therefore, the mixing model includes the mineralization of these water types from the areas where they were defined to the center of mass of the study site. LSW, the WT that is closest to its formation area, has the lowest AOU$_i$, while the high AOU$_i$ of LDW indicates that the area where it was defined, in the Vema Channel at 11°N (see Table S1), is furthest away from the study area and basin-scale mineralization has occurred. For the inorganic nutrients, the molar N:P ratio of these water types is 15 ± 1 (Table 1), very similar to the canonical Redfield ratio of 16.

[31] The WT values of the MW are not included here because the average proportion of this WT in the study area is so small (~4%; Figure 3a, see Table S1) that the estimated WT values have unacceptably high errors.

4.3. Impact of Conservative Mixing Versus Nonconservative Biogeochemical Processes on Organic Carbon and Nutrients

[32] For the organic carbon and nutrients, the total variability explained by the mixing model is much lower, ranging from 18–63% (Table 1), indicating a higher influence of local metabolic activity on the variability of dissolved organic

Table 2. Mixing-Biogeochemical Model of Chemical and Biological Parameters Taking the Proportions of the Water Masses into Account[a]

N_1[b]	N_2[b]	Unit	r^{2c}	SD[d]	n[e]	$\beta \pm SE$[f]	p[g]
AOU	PO_4	Molar ratio	0.98	3.2	113	126 ± 11	< 0.0001
AOU	NO_3	Molar ratio	0.98	2.7	113	9.7 ± 0.6	< 0.0001
NO_3	PO_4	Molar ratio	0.99	0.2	113	13.0 ± 0.7	< 0.0001
DOC	AOU	Molar ratio					ns
DON	AOU	Molar ratio					ns
DOP	AOU	Molar ratio					ns
PA	NO_3	cells $\mu mol^{-1} kg^{-1}$					ns
PA	PO_4	cells $\mu mol^{-1} kg^{-1}$	0.80	0.17	104	4.5 ± 2.0[h]	0.0260
PA	DOC	cells $\mu mol^{-1} kg^{-1}$					ns
PA	DON	cells $\mu mol^{-1} kg^{-1}$	0.78	0.17	96	-0.3 ± 0.2[h]	0.0354
PA	DOP	cells $\mu mol^{-1} kg^{-1}$					ns
HNA	PA	Ratio	0.99	0.03[h]	104	0.82 ± 0.02	< 0.0001
PHP	PB	d^{-1}	0.70	0.29	90	0.023 ± 0.005	< 0.0001

[a]For relationships of water mass modeled parameters according to equation (1) and the residual parameters according to equation (2), see Figure S3 and S4.
[b]Chemical and biological parameters; Abbreviations of N_1 and N_2 see text.
[c]Adjusted coefficient of determination.
[d]Standard deviation of the residuals of the model.
[e]Number of data points.
[f]Beta coefficients (β) and standard error (SE) of the multiple regression analysis based on the residuals of chemical and biological parameters (N_i) and the proportions of the water masses derived from the mixing model applying equation (2).
[g]p value indicating significant regression model; ns indicates regression model not significant.
[h]Number $\times 10^5$.

matter [*McCarthy et al.*, 1998]. As the SD of DOP is similar to the analytical error, this variable was not used for any further calculations. The DOC:DON ratio of the WT range between 16 ± 3 and 17 ± 3 for the LSW and LDW, respectively (Table 1). A much lower DOC:DON ratio of 8 ± 1 was found in the ISOW, resembling the C:N ratio of fresh phytoplankton-derived organic matter, consistent with the relatively higher PHP and turnover rate in this SWT compared to the LSW and LDW (Table 1).

4.4. Impact of Conservative Mixing Versus Nonconservative Biogeochemical Processes on Microbial Activity

[33] Between 64–79% of the total variability in prokaryotic abundance, including HNA cells and PHP, was explained by conservative mixing (Table 1). Therefore, a notably large fraction of the variability, ranging from 21–36%, was explained by the local biological activity (see Var% in Table 1). This might indicate that a resident prokaryotic community exists that is typical for the NEADW, as has been shown by *Agogué et al.* [2010]. Similar to the nutrient analyses, the fraction of variability in prokaryotic abundance, HNA and PHP that is not accounted for by equation (1), is interpreted as the variability due to nonconservative biogeochemical processes. Analytical and sampling errors might also contribute to this residual variability. However, if the variability would be exclusively due to analytical and sampling errors, then the values of β would not be statistically significant and would produce unrealistic values.

4.5. Variability of Nutrient Ratios

[34] It is commonly assumed that sinking particulate organic matter (POM) fuels heterotrophic activity in the dark ocean [*Arístegui et al.*, 2009] and that the particles are solubilized by prokaryotes before the organic matter is utilized for biomass production, respiration, and energy acquisition [*Baltar et al.*, 2009]. There is evidence that an abundant particle-attached microbial community exists in the deep ocean [*Moeseneder et al.*, 2001; *Lauro and Bartlett*, 2008]

providing substrate for pelagic microbes [*Karl et al.*, 1988] and leading to a preferential removal of N- and P-containing organic compounds [*Schneider*, 2003]. However, recent studies suggest that surface derived organic matter might not be enough to fuel the metabolism of heterotrophic prokaryotes in the dark ocean [*Reinthaler et al.*, 2006; *Baltar et al.*, 2009].

[35] When using equation (2) and applying $N_1 = $ AOU and $N_2 = NO_3$ (or PO_4), then β yields the stoichiometric coefficient of dissolved oxygen consumption to inorganic nitrogen (or phosphorus) production. Considering the values and the standard errors of these β coefficients (Table 2), the modeled O_2:N:P ratios independent of the mixing within the NEADW core of 126($\pm$11):13.0 ($\pm$0.7):1 are in good agreement with earlier studies from similar depths [*Anderson and Sarmiento*, 1994]. From the β coefficients, we calculated the contribution of the different biomolecules to the oxygen consumed in the NEADW. Following the approach of *Fraga et al.* [1998] (see supporting information Materials and Methods), the material mineralized in the NEADW averaged over the transect was composed of $14 \pm 3\%$ of phosphorus compounds, $43 \pm 8\%$ of proteins, and $43 \pm 11\%$ of carbohydrates and lipids. This yields a C:N:P composition of the mineralized biogenic material in the NEADW of 87–96:13:1. This suggests a preferential (but not significant) mineralization of phosphorus compounds when compared to the classical surface Redfield ratio of 106:16:1.

[36] Applying $N_1 = $ AOU and $N_2 = $ DOC to equation (2) and dividing β by the AOU:C_{org} stoichiometric molar ratio which ranges from 1.31 to 1.44, depending on the possible relative proportions of consumed carbohydrates and lipids (see section 2.7 and supporting information Materials and Methods), yields the contribution of dissolved organic matter to oxygen consumption. The importance of DOM export from the surface ocean has only recently been recognized and is estimated to contribute about 20% of the total organic carbon flux to the global dark ocean [*Hansell et al.*, 2012]. Using a high-resolution DOC data set and a different modeling approach, *Carlson et al.* [2010] calculated that DOC
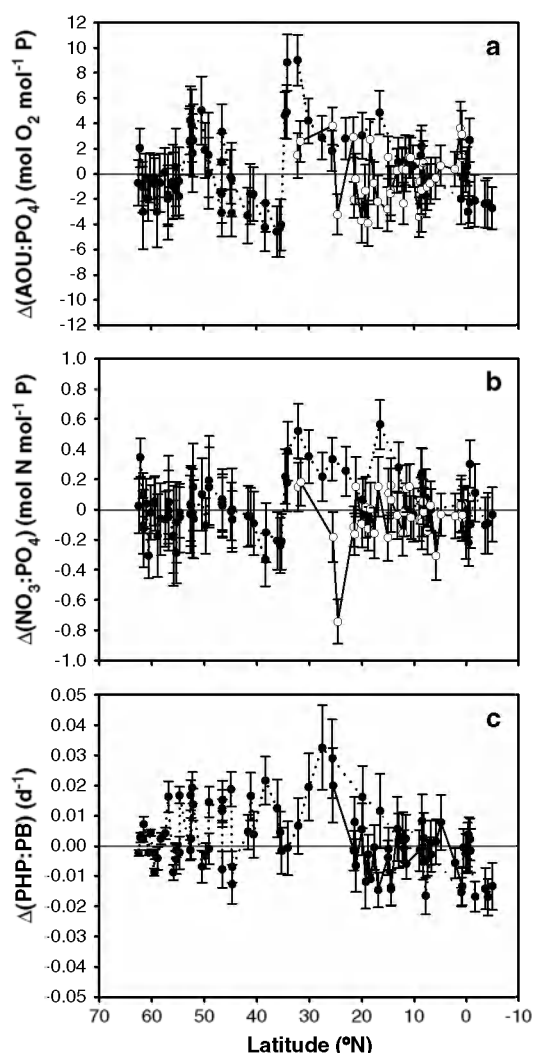
Figure 6. Meridional changes in the modeled (a) Δ(AOU: PO_4) ratios and (b) Δ(NO_3:PO_4). Negative anomalies indicate the mineralization of younger organic matter; positive anomalies indicate the mineralization of older organic matter. (c) Modeled prokaryotic growth rates Δ(PHP:PB) along the transect. Black dots connected with lines indicate the stations occupied along the MAR, white circles connected with dashed lines indicate stations off the shelf of Africa. Error bars indicate the standard deviations from the perturbation analysis.

export contributes about 9–19% to the oxygen consumption in the NEADW. We found no significant relationships of the AOU to DOC, DON, and DOP once the effect of water masses mixing and basin-scale mineralization was removed (Table 2), indicating that heterotrophic mineralization of the resident DOM is not the main driver of local oxygen consumption in the NEADW. Comparing the SWT mixing model values of AOU and DOC for LSW ($15 \pm 4\,\mu$mol $O_2\,kg^{-1}$ and $60 \pm 4\,\mu$mol $C\,kg^{-1}$, respectively) and LDW ($118 \pm 3\,\mu$mol $O_2\,kg^{-1}$ and $45 \pm 3\,\mu$mol $C\,kg^{-1}$, respectively), a DOC to AOU ratio of -0.16 ± 0.05 mol C mol^{-1} O_2 can be obtained. Considering the AOU:C_{org} molar ratio of 1.31–1.44 presented above suggests that the maximum possible contribution of DOC to the basin scale oxygen

consumption of the deep eastern North Atlantic Ocean is about $20 \pm 7\%$, which is at the upper end of the estimate by *Carlson et al.* [2010]. It should be noted that we reached this conclusion using an independent methodology—the water type values of DOC and AOU from a multiparameter water mass analysis—indicating that the oxygen consumption occurred within the WT from the areas where they were defined to the study site. From the β values of the AOU/DOC, AOU/DON, and AOU/DOP pairs, it is clear, however, that at the local scale, the particulate fraction plays a more important role in the organic matter pool utilized by prokaryotes as supported by previous findings. Recently, evidence has been presented that in the deep North Atlantic, the POC concentration and the deep-water heterotrophic microbial activity are tightly linked [*Baltar et al.*, 2009]. Also, *Bochdansky et al.* [2010] showed that layers of high-particle concentrations are linked to oxygen anomalies. The fraction of fast sinking to buoyant POM potentially available to prokaryotes, however, remains to be determined.

[37] The SD of the estimation performed with the mixing-biogeochemical inverse models obtained with equation (2) (Table 2) is significantly better than the estimations based on the mixing model calculated using equation (1) alone (Table 1). For example, the SD of AOU decreased from $4.8\,\mu$mol $O_2\,kg^{-1}$ with the mixing model to 2.7 (or 3.3 μmol $O_2\,kg^{-1}$) with the mixing-biogeochemical model including NO_3 (or PO_4). However, this SD is still larger than the analytical error of the determination of AOU. In fact, an analysis of the distribution of the residuals of equation (2) (i.e., ΔN_{1j}) along the latitude and longitude in the NE Atlantic indicates that the distribution of those residuals is not random (Figure 6). This is an indication that the coupled mixing-biogeochemical model is still insufficient to explain all the observed variability. For $N_1 = $ AOU and $N_2 = NO_3$ (or PO_4), a biased distribution of $\Delta(N_{1j}:N_{2j})$ shows deviations from the average AOU:N (or N:P) stoichiometric coefficients of 9.7 ± 0.6 (or 13.0 ± 0.7) obtained with equation (2) (Table 2). We interpret these deviations as an indication of changes in the biogeochemical composition of the mineralized materials with latitude and/or longitude. The Δ(AOU: PO_4) ratios (Figure 6a) are negative to up to -5 mol O_2 mol^{-1} P in the temperate region between 45°N and 35°N (average $\pm$ sd of Δ(AOU:PO_4) $= -2.7 \pm 1.6$ mol O_2 mol^{-1} P, $n = 11$) suggesting the mineralization of fresher POM below the transition zone between the North Atlantic Current and the Azores Current. According to *Kahru et al.* [1991], higher productivity and fast sinking rates of large-size fresh POM are common in this area. In contrast, the positive Δ(AOU:PO_4) ratios near the Charlie-Gibbs Fracture Zone, between 55°N and 45°N (average $\pm$ sd of Δ(AOU:PO_4) $= +1.0 \pm 2.3$ mol O_2 mol^{-1} P, $n = 20$) and particularly under the subtropical gyre, from 35°N to 15°N (average $\pm$ sd of Δ(AOU:PO_4) $= 4.3 \pm 2.4$ mol O_2 mol^{-1} P, $n = 13$) point to the mineralization of relatively aged sinking material. This coincides with the inflow of LSW in the CGFZ and the low productivity in the oligotrophic surface waters of the subtropical gyre with its presumed low flux of predominantly small slow-sinking particles into the dark ocean.

[38] In the subtropical Atlantic region, we followed the NEADW along the MAR and along a transect closer to the shelf off the African continent ($\sim$600 km from the coastline) (Figure 1). There, the range of the Δ(AOU:PO_4) ratio was

narrower with predominantly lower values than the average AOU:PO$_4$ (average ± sd of Δ(AOU:PO$_4$) = −0.5 ± 2.1 mol O$_2$ mol^{-1} P, n = 31), suggesting that lateral transport from the shelf region due to filaments and from the NW African eastern boundary upwelling system introduces fresh POM into the NEADW [*Arístegui et al.*, 2003]. A similar trend is observed in the open ocean south of 15°N, i.e., in the area under the influence of the North Equatorial Current, which also transports fresh material from the African coast (average ± sd of Δ(AOU:PO$_4$) = −0.5 ± 1.7 mol O$_2$ mol^{-1} P, n = 21) and for the residuals of the Δ(NO$_3$:PO$_4$) ratios (Figure 6b).

4.6. Prokaryotic Activity in the NEADW

[39] An increasing fraction of high nucleic acid (HNA)-containing prokaryotes from the epipelagic to the bathypelagic ocean has been reported previously [*Reinthaler et al.*, 2006; *Gasol et al.*, 2009]. HNA bacteria have been shown to be more active suggesting that HNA cells are metabolically more versatile than LNA cells [*Gasol et al.*, 1999]. *Bouvier et al.* [2007] hypothesized that HNA- and LNA-containing bacteria might be phylogenetically different communities. Recently, the notion of distinct HNA- and LNA-containing bacterial groups has been corroborated using 16S rRNA pyrosequencing and fluorescence in situ hybridization (FISH) [*Schattenhofer et al.*, 2011; *Vila-Costa et al.*, 2012]. These surface ocean studies revealed that the HNA fraction is composed of mostly versatile and fast-growing bacteria such as the SAR324 and SAR406 clusters, members of the Deltaproteobacteria and Fibrobacteres. Interestingly, *Agogué et al.* [2010] found that members of the SAR324 and SAR406 cluster are substantially more abundant in the LSW and NEADW along a similar transect as covered in this study. FISH analysis of the prokaryotic community along a transect in the North Atlantic showed that Archaea contribute up to 20% of the picoplankton in the NEADW and constitute a metabolically active group [*Teira et al.*, 2006; *Varela et al.*, 2007]. With conventional flow cytometric counting using fluorescent labels to stain prokaryotes, however, it is currently not possible to separate the bacterial and archaeal contribution to the total abundance of the dark ocean prokaryotic community.

[40] Several lines of evidence suggest that the fraction of HNA-containing cells are indeed the more active component in the NEADW. First, the variability of the residuals of prokaryotic abundance is essentially explained by the variability of the residuals of HNA cells: The r^2 of the mixing model of HNA cells increases from 0.76 to 0.99 when prokaryotic abundance is included as explanatory variable in the mixing-biogeochemistry model (compare Table 1 and Table 2), indicating that the changes in abundance occur in the HNA fraction. Concomitantly, the SD of the estimated HNA cells decreases from 0.14 × 10^5 to 0.03 × 10^5 cells mL^{-1}. Second, there is a positive relationship between the residuals of PHP and the residuals of PB (Table 2); the r^2 of the mixing model of PHP increases from 0.64 to 0.70 when PB is included as explanatory variable in the mixing-biogeochemistry model and the SD of estimated PHP decreases from 0.31 nmol C L^{-1} d^{-1} in the mixing model to 0.29 nmol C L^{-1} d^{-1} in the mixing-biogeochemical model including PB as explanatory variable (compare Table 1 and Table 2). This, in turn, indicates that any increase in PHP that is not explained by mixing must

be due to a higher activity of a fraction of the cells found in the NEADW that according to the value of β when N_1 = PHP and N_2 = PB, exhibits a mean growth rate of 0.023 ± 0.005 d^{-1} or a generation time of 43 ± 10 d (Table 2).

[41] There is uncertainty in our measurements of PHP and PB. Biases of prokaryotic activity due to pressure effects have not yet been unequivocally shown [*Tamburini et al.*, 2013] and the conversion factor between leucine incorporation and cell abundance into units of carbon might be different for the more productive northern North Atlantic and the subtropical gyre region [*Alonso-Sáez et al.*, 2007]. *Del Giorgio et al.* [2011] conducted a study comparing the relationships between long-term versus short-term incubations of PHP with calculated growth efficiencies. Their data suggest that empirically derived conversion factors from short-term incubations might be underestimates. Furthermore, a conversion factor of ~1.5 kg C mol Leu^{-1} was required to balance the carbon budget in the Ross Sea of the Southern Ocean [*Ducklow et al.*, 2000]. Thus, there are strong indications that our chosen theoretical conversion factor of 1.5 kg C mol Leu^{-1} yields reasonable estimates of PHP.

[42] Figure 6c shows that Δ(PHP:PB) is not homogeneously distributed with latitude and longitude: the average ± sd of Δ(PHP:PB) is +0.004 ± 0.009 d^{-1} (n = 41) below the subpolar-temperate eastern North Atlantic (65°N–35°N), increasing significantly to +0.019 ± 0.007 d^{-1} (n = 7) below the subtropical gyre (35°N–15°N) and then, decreasing significantly to −0.005 ± 0.008 d^{-1} (n = 18) within the North Equatorial Current domain south of 15°N. Finally, in the area under the influence of the Canary current eastern boundary upwelling system, values of Δ(PHP:PB) significantly lower than the average PHP:PB were also observed (−0.003 ± 0.007 d^{-1}; n = 24). This indicates that the highly active heterotrophic prokaryotes below the subtropical gyre turn over significantly faster (~24 days) than those below the subpolar–temperate North Atlantic (~37 days). However, the turnover time of heterotrophic prokaryotes below the areas influenced by the upwelling of the Canary Current (~55 days) and the North Equatorial Current (~50 days) is significantly longer than those below the subtropical gyre. Relatively short prokaryotic turnover times below the subtropical gyre region are counterintuitive. One would expect higher growth rates or shorter turnover times where the prokaryotic substrate is supposedly fresh due to recent water mass formation or below regions where our model indicates vertical input of fresher surface-derived material. Measured PHP and PA clearly show a latitudinal trend with higher growth rates in the northern parts of the NEADW than under the North Atlantic gyre system [*Reinthaler et al.*, 2006]. Whether these relatively high turnover rates of prokaryotes in the NEADW of the subtropical Atlantic are a genuine feature or are caused by changing conversion factors used in the calculations of PB and PHP, require further investigation.

4.7. Concluding Comments

[43] In the NEADW, most of the nutrient concentrations are influenced by the input from water masses above and below the deep North Atlantic salinity maximum indicating that mixing processes are mainly responsible for the observed latitudinal changes in the nutrient concentrations in the NEADW. The mixing-corrected mineralization ratios in the NEADW indicate a major contribution of particulate organic

matter serving as substrate for the heterotrophic prokaryotes, while the maximum contribution of dissolved organic carbon to the oxygen consumption is about 20%. In contrast to the inorganic and organic matter, biological activity behaves differently and the relatively high activity in the NEADW is less influenced by mixing than the inorganic nutrient concentrations.

[44] Mixing and mineralization processes from the WT formation sites explained 64% of the variability in PHP. Considering our reported turnover times ranging from 100 to 800 days suggest that dark ocean microbial activity is representative for relatively long-time periods. Thus, the area of WT origin dictate the contrasting initial values of PB and PHP. Conversely, 36% of the variability of PHP was associated with local mineralization of sinking POM which is the substrate for an active fraction of the prokaryotic community with a turnover of just 43 ± 10 days. Thus, we were able to show that the local-scale variability of dissolved oxygen and nutrients is mainly led by microbial mineralization of sinking particles and, consequently, that both the local nutrient mineralization and local microbial activity can occur at comparable time scales.

[45] The latitudinal variability of the nutrient ratios and the prokaryotic turnover suggests a dependence on the biogeochemical province crossed by the NEADW core. Hence, to decipher the mineralization and the prokaryotic activity in the dark ocean, the mixing of water masses and the surface processes in the biogeochemical provinces need to be taken into account.

References

Agogué, H., D. Lamy, P. R. Neal, M. L. Sogin, and G. J. Herndl (2010), Water mass-specificity of bacterial communities in the North Atlantic revealed by massively parallel sequencing, *Mol. Ecol.*, 20(2), 258–274, doi:10.1111/j.1365-294X.2010.04932.x.

Alonso-Sáez, L., J. M. Gasol, J. Arístegui, J. C. Vilas, D. Vaque, C. M. Duarte, and S. Agusti (2007), Large-scale variability in surface bacterial carbon demand and growth efficiency in the subtropical northeast Atlantic Ocean, *Limnol. Oceanogr.*, 52(2), 533–546.

Alvarez, M., F. F. Perez, H. Bryden, and A. F. Rios (2004), Physical and biogeochemical transports structure in the North Atlantic subpolar gyre, *J. Geophys. Res.*, 109, C03027, doi:10.1029/2003JC002015.

Álvarez-Salgado, X. A., M. Nieto-Cid, J. Gago, S. Brea, C. G. Castro, M. D. Doval, and F. F. Pérez (2006), Stoichiometry of the degradation of dissolved and particulate biogenic organic matter in the NW Iberian upwelling, *J. Geophys. Res.*, 111, C07017, doi:10.1029/2004JC002473.

Álvarez-Salgado, X. A., M. Nieto-Cid, M. Álvarez, F. F. Pérez, P. Morin, and H. Mercier (2013), New insights on the mineralization of dissolved organic matter in central, intermediate and deep water masses of the northeast North Atlantic, *Limnol. Oceanogr.*, 58, 681–696.

Anderson, L., and J. L. Sarmiento (1994), Redfield ratios of remineralization determined by nutrient data analysis, *Global Biogeochem. Cycles*, 8(1), 65–80.

Arístegui, J., C. M. Duarte, S. Agusti, M. Doval, X. A. Álvarez-Salgado, and D. A. Hansell (2002), Dissolved organic carbon support of respiration in the dark ocean, *Science*, 298(5600), 1967, doi:10.1126/science.1076746.

Arístegui, J., E. Barton, M. Montero, M. García-Muñoz, and J. Escánez (2003), Organic carbon distribution and water column respiration in the NW Africa-Canaries Coastal Transition Zone, *Aquat. Microb. Ecol.*, 33, 289–301.

Arístegui, J., J. M. Gasol, C. M. Duarte, and G. J. Herndl (2009), Microbial oceanography of the dark ocean's pelagic realm, *Limnol. Oceanogr.*, 54(5), 1501–1529, doi:10.1029/2002JC001625.

Baltar, F., J. Arístegui, J. M. Gasol, E. Sintes, and G. J. Herndl (2009), Evidence of prokaryotic metabolism on suspended particulate organic matter in the dark waters of the subtropical North Atlantic, *Limnol. Oceanogr.*, 54(1), 182–193.

Bauer, J., P. Williams, and E. R. M. Druffel (1992), C-14 activity of dissolved organic carbon fractions in the north-central Pacific and Sargasso Sea, *Nature*, 357(6380), 667–670.

Bendtsen, J., C. Lundsgaard, M. Middelboe, and D. Archer (2002), Influence of bacterial uptake on deep-ocean dissolved organic carbon, *Global Biogeochem. Cycles*, 16(4), 1127, doi:10.1029/2002GB001947.

Bochdansky, A. B., H. M. van Aken, and G. J. Herndl (2010), Role of macroscopic particles in deep-sea oxygen consumption, *Proc. Natl. Acad. Sci. U. S. A.*, 107(18), 8287–8291, doi:10.1073/pnas.0913744107.

Bouvier, T., P. A. del Giorgio, and J. M. Gasol (2007), A comparative study of the cytometric characteristics of high and low nucleic-acid bacterioplankton cells from different aquatic ecosystems, *Environ. Microbiol.*, 9(8), 2050–2066, doi:10.1111/j.1462-2920.2007.01321.x.

Brea, S., X. A. Álvarez-Salgado, M. Alvarez, F. Perez, L. Memery, H. Mercier, and M. Messias (2004), Nutrient mineralization rates and ratios in the eastern South Atlantic, *J. Geophys. Res.*, 109, C05030, doi:10.1029/2003JC002051.

Bryden, H. L., H. R. Longworth, and S. A. Cunningham (2005), Slowing of the Atlantic meridional overturning circulation at 25°N, *Nature*, 438(7068), 655–657, doi:10.1038/nature04385.

Burd, A. B., et al. (2010), Assessing the apparent imbalance between geochemical and biochemical indicators of meso- and bathypelagic biological activity What the @$#! is wrong with present calculations of carbon budgets?, *Deep Sea Res., Part II*, 57(16), 1557–1571, doi:10.1016/j.dsr2.2010.02.022.

Carlson, C. A., D. A. Hansell, N. B. Nelson, D. A. Siegel, W. M. Smethie, S. Khatiwala, M. M. Meyers, and E. Halewood (2010), Dissolved organic carbon export and subsequent remineralization in the mesopelagic and bathypelagic realms of the North Atlantic basin, *Deep Sea Res., Part II*, 57(16), 1433–1445, doi:10.1016/j.dsr2.2010.02.013.

del Giorgio, P. A., R. Condon, T. Bouvier, K. Longnecker, C. Bouvier, E. Sherr, and J. M. Gasol (2011), Coherent patterns in bacterial growth, growth efficiency, and leucine metabolism along a northeastern Pacific inshore-offshore transect, *Limnol. Oceanogr.*, 56(1), 1–16, doi:10.4319/lo.2011.56.1.0001.

Ducklow, H., M. Dickson, D. Kirchman, G. F. Steward, J. Orchardo, J. Marra, and F. Azam (2000), Constraining bacterial production, conversion efficiency and respiration in the Ross Sea, Antarctica, January–February, 1997, *Deep Sea Res., Part II*, 47(15-16), 3227–3247.

Fraga, F., A. Rios, F. Perez, and F. Figueiras (1998), Theoretical limits of oxygen:carbon and oxygen:nitrogen ratios during photosynthesis and mineralisation of organic matter in the sea, *Sci. Mar.*, 62(1-2), 161–168.

Gasol, J. M., U. L. Zweifel, F. Peters, J. A. Fuhrman, and Å. Hagstroem (1999), Significance of size and nucleic acid content heterogeneity as measured by flow cytometry in natural planktonic bacteria, *Appl. Environ. Microbiol.*, 65(10), 4475–4483.

Gasol, J. M., L. Alonso-Sáez, D. Vaque, F. Baltar, M. L. Calleja, C. M. Duarte, and J. Arístegui (2009), Mesopelagic prokaryotic bulk and single-cell heterotrophic activity and community composition in the NW Africa–Canary Islands coastal-transition zone, *Prog. Oceanogr.*, 83(1–4), 189–196, doi:10.1016/j.pocean.2009.07.014.

Gordon, L., J. Jennings Jr., and A. Ross (1993), A suggested protocol for continuous flow automated analysis of seawater nutrients (phosphate, nitrate, nitrite and silicic acid) in the WOCE Hydrographic Program and the Joint Global Ocean Fluxes Study, *Methods Manual WHPO*, 91-1, 55.

Hansell, D. A. (2013), Recalcitrant dissolved organic carbon fractions, *Annu. Rev. Mar. Sci.*, 5, 421–445.

Hansell, D. A., and C. A. Carlson (2001), Biogeochemistry of total organic carbon and nitrogen in the Sargasso Sea: Control by convective overturn, *Deep Sea Res., Part II*, 48, 1649–1667.

Hansell, D. A., C. A. Carlson, D. Repeta, and R. Schlitzer (2009), Dissolved organic matter in the ocean, *Oceanography*, 20(4), 202–211.

Hansell, D. A., C. A. Carlson, and R. Schlitzer (2012), Net removal of major marine dissolved organic carbon fractions in the subsurface ocean, *Global Biogeochem. Cycles*, 26, GB1016, doi:10.1029/2011GB004069.

Herndl, G. J., T. Reinthaler, E. Teira, H. M. van Aken, C. Veth, A. Pernthaler, and J. Pernthaler (2005), Contribution of Archaea to total prokaryotic production in the deep Atlantic Ocean, *Appl. Environ. Microbiol.*, 71(5), 2303–2309, doi:10.1128/AEM.71.5.2303-2309.2005.

Jannasch, H., and C. Taylor (1984), Deep-sea microbiology, *Annu. Rev. Microbiol.*, 38(1), 487–487.

Kahru, M., S. Nômmann, and B. Zeitzschel (1991), Particle (Plankton) size structure across the Azores Front (Joint Global Ocean Flux Study North Atlantic bloom experiment), *J. Geophys. Res.*, *96*, 7083–7088.

Karl, D., G. Knauer, and J. Martin (1988), Downward flux of particulate organic matter in the ocean—A particle decomposition paradox, *Nature*, *332*(6163), 438–441.

Kramer, G., C. Pausz, and G. J. Herndl (2005), Elemental composition of dissolved organic matter and bacterioplankton production in the Faroe-Shetland Channel (North Atlantic), *Deep Sea Res., Part II*, *52*(1), 85–97, doi:10.1016/j.dsr.2004.09.002.

Lauro, F. M., and D. H. Bartlett (2008), Prokaryotic lifestyles in deep sea habitats, *Extremophiles*, *12*(1), 15–25, doi:10.1007/s00792-006-0059-5.

Lawson, C. L., and R. J. Hanson (Eds) (1974), *Solving Least Squares Problems*, Prentice-Hall, Englewood Cliffs, N. J.

Li, Y., and T. Peng (2002), Latitudinal change of remineralization ratios in the oceans and its implication for nutrient cycles, *Global Biogeochem. Cycles*, *16*(4), 1130, doi:10.1029/2001GB001828.

Mantyla, A. W. (1994), The treatment of inconsistencies in Atlantic deep-water salinity data, *Deep Sea Res., Part I*, *41*(9), 1387–1405.

McCarthy, M. D., J. Hedges, and R. Benner (1998), Major bacterial contribution to marine dissolved organic nitrogen, *Science*, *281*(5374), 231–234.

Moeseneder, M., C. Winter, and G. Herndl (2001), Horizontal and vertical complexity of attached and free-living bacteria of the eastern Mediterranean Sea, determined by 16S rDNA and 16S rRNA fingerprints, *Limnol. Oceanogr.*, *46*(1), 95–107.

Nagata, T., H. Fukuda, R. Fukuda, and I. Koike (2000), Bacterioplankton distribution and production in deep Pacific waters: Large-scale geographic variations and possible coupling with sinking particle fluxes, *Limnol. Oceanogr.*, *45*(2), 426–435.

Nagata, T., et al. (2010), Emerging concepts on microbial processes in the bathypelagic ocean—Eecology, biogeochemistry, and genomics, *Deep Sea Res., Part II*, *57*(16), 1519–1536, doi:10.1016/j.dsr2.2010.02.019.

Paillet, J., and H. Mercier (1997), An inverse model of the eastern North Atlantic general circulation and thermocline ventilation, *Deep Sea Res., Part I*, *44*(8), 1293–1328.

Perez, F., C. Mouriño, F. Fraga, and A. Rios (1993), Displacement of water masses and remineralization rates off the Iberian Peninsula by nutrient anomalies, *J. Mar. Res.*, *51*(4), 869–892.

Reid, J. L. (1994), On the total geostrophic circulation of the South Atlantic Ocean: Flow patterns, tracers, and transports, *Prog. Oceanogr.*, *23*(3), 1–92.

Reinthaler, T., H. M. van Aken, C. Veth, J. Arístegui, C. Robinson, P. J. L. B. Williams, P. Lebaron, and G. J. Herndl (2006), Prokaryotic respiration and production in the meso-and bathypelagic realm of the eastern and western North Atlantic basin, *Limnol. Oceanogr.*, *51*(3), 1262–1273.

Reinthaler, T., H. M. van Aken, and G. J. Herndl (2010), Major contribution of autotrophy to microbial carbon cycling in the deep North Atlantic's interior, *Deep Sea Res., Part II*, *57*(16), 1572–1580, doi:10.1016/j.dsr2.2010.02.023.

Schattenhofer, M., J. Wulf, I. Kostadinov, F. O. Glöckner, M. V. Zubkov, and B. M. Fuchs (2011), Phylogenetic characterisation of picoplanktonic populations with high and low nucleic acid content in the North Atlantic Ocean, *Syst. Appl. Microbiol.*, *34*(6), 470–475, doi:10.1016/j.syapm.2011.01.008.

Schlitzer, R. (2002), Interactive analysis and visualization of geoscience data with Ocean Data View, *Comput. Geosci.*, *28*(10), 1211–1218.

Schneider, B. (2003), Depth-dependent elemental compositions of particulate organic matter (POM) in the ocean, *Global Biogeochem. Cycles*, *17*(2), 1032, doi:10.1029/2002GB001871.

Schneider, B., J. Karstensen, A. Oschlies, and R. Schlitzer (2005), Model-based evaluation of methods to determine C:N and N:P regeneration ratios from dissolved nutrients, *Global Biogeochem. Cycles*, *19*, GB2009, doi:10.1029/2004GB002256.

Shaffer, G., J. Bendtsen, and O. Ulloa (1999), Fractionation during remineralization of organic matter in the ocean, *Deep Sea Res., Part I*, *46*(2), 185–204.

Simon, M., and F. Azam (1989), Protein content and protein synthesis rates of planktonic marine bacteria, *Mar. Ecol. Prog. Ser.*, *51*(3), 201–213.

Smethie, W., R. Fine, A. Putzka, and E. Jones (2000), Tracing the flow of North Atlantic Deep Water using chlorofluorocarbons, *J. Geophys. Res.*, *105*(C6), 14,297–14,323.

Steinberg, D. K., B. A. S. Van Mooy, K. O. Buesseler, P. W. Boyd, T. Kobari, and D. M. Karl (2008), Bacterial vs. zooplankton control of sinking particle flux in the ocean's twilight zone, *Limnol. Oceanogr.*, *53*(4), 1327–1338.

Takahashi, T., W. S. Broecker, and S. Langer (1985), Redfield ratio based on chemical data from isopycnal surfaces, *J. Geophys. Res.*, *90*(C4), 6907–6924.

Tamburini, C., M. Boutrif, M. Garel, R. R. Colwell, and J. W. Deming (2013), Prokaryotic responses to hydrostatic pressure in the ocean—A review, *Environ. Microbiol.*, *15*(5), 1262–1274, doi:10.1111/1462-2920.12084.

Teira, E., P. Lebaron, H. M. van Aken, and G. J. Herndl (2006), Distribution and activity of bacteria and archaea in the deep water masses of the North Atlantic, *Limnol. Oceanogr.*, *51*(5), 2131–2144.

Turley, C. M. (1993), The effect of pressure on leucine and thymidine incorporation by free-living bacteria and by bacteria attached to sinking oceanic particles, *Deep Sea Res., Part I*, *40*, 2193–2206.

van Aken, H. M. (2000), The hydrography of the mid-latitude northeast Atlantic Ocean I: The deep water masses, *Deep Sea Res., Part I*, *47*(5), 757–788.

Varela, M. M., H. M. van Aken, E. Sintes, and G. J. Herndl (2007), Latitudinal trends of Crenarchaeota and Bacteria in the meso- and bathypelagic water masses of the Eastern North Atlantic, *Environ. Microbiol.*, *10*(1), 110–124.

Vila-Costa, M., J. M. Gasol, S. Sharma, and M. A. Moran (2012), Community analysis of high- and low-nucleic acid-containing bacteria in NW Mediterranean coastal waters using 16S rDNA pyrosequencing, *Environ. Microbiol.*, *14*(6), 1390–1402, doi:10.1111/j.1462-2920.2012.02720.x.

Williams, P. M., and E. R. M. Druffel (1987), Radiocarbon in dissolved organic matter in the central North Pacific Ocean, *Nature*, *330*, 246–248.

WOCE operations manual (1994), WOCE Hydrographic Program Office Rep. WHPO 91-1, WOCE Rep. 68/91.